doi:10.1016/j.jmb.2005.08.057 J. Mol. Biol. (2005) 353, 655–663

JMB

Available online at www.sciencedirect.com

SCIENCE DIRECT®

ELSEVIER

Crystal Structure of Methyl Parathion Hydrolase from *Pseudomonas* sp. WBC-3

Yan-Jie Dong[1,3]†, Mark Bartlam[2,4]†, Lei Sun[2,4], Ya-Feng Zhou[1] Zhi-Ping Zhang[1], Cheng-Gang Zhang[3], Zihe Rao[2,4]* and Xian-En Zhang[1,2]*

[1]*Joint Research Group on Analytical Biotechnology of Institute of Biophysics and Wuhan Institute of Virology Chinese Academy of Sciences Beijing 100101, China*

[2]*National Laboratory of Biomacromolecules and National Laboratory of Virology Institute of Biophysics, Chinese Academy of Science, Beijing 100101, China*

[3]*Shenyang Institute of Applied Ecology, Chinese Academy of Sciences, Shenyang 110015 China*

[4]*Laboratory of Structural Biology, Tsinghua University Beijing 100084, China*

**Corresponding authors*

Methyl parathion hydrolase (MPH, E.C.3.1.8.1), isolated from the soil-dwelling bacterium *Pseudomonas* sp. WBC-3, is a Zn(II)-containing enzyme that catalyzes the degradation of the organophosphate pesticide methyl parathion. We have determined the structure of MPH from *Pseudomonas* sp. WBC-3 to 2.4 Å resolution. The enzyme is dimeric and each subunit contains a mixed hybrid binuclear zinc center, in which one of the zinc ions is replaced by cadmium. In both subunits, the more solvent-exposed β-metal ion is substituted for Cd^{2+} due to high cadmium concentration in the crystallization condition. Both ions are surrounded by ligands in an octahedral arrangement. The ions are separated by 3.5 Å and are coordinated by the amino acid residues His147, His149, Asp151, His152, His234 and His302 and a water molecule. Asp255 and a water molecule serve to bridge the zinc ions together. MPH is homologous with other metallo-β-lactamases but does not show any similarity to phosphotriesterase that can also catalyze the degradation of methyl parathion with lower rate, despite the lack of sequence homology. Trp179, Phe196 and Phe119 form an aromatic cluster at the entrance of the catalytic center. Replacement of these three amino acids by alanine resulted in a significant increase of K_m and loss of catalytic activity, indicating that the aromatic cluster has an important role to facilitate affinity of enzyme to the methyl parathion substrates.

Keywords: methyl parathion hydrolase; crystal structure; binuclear metal center; metallo-β-lactamase; organophosphate pesticides

Introduction

Organophosphate pesticides such as parathion (*O*,*O*-diethyl *O*-*p*-nitrophenylphosphorothioate) and methyl parathion (*O*,*O*-dimethyl *O*-*p*-nitrophenylphosphorothioate, MP) are highly toxic agricultural chemicals that are still used extensively worldwide to control a wide range of insect species. The biodegradation of organophosphate agents has been widely studied for their high toxicity to the environment and animal health.[1–6] Organophosphorus hydrolases (OPH, E.C.3.1.8) play important roles in the decontamination of organophosphate pesticides and are useful in the bioremediation of pollution caused by these pesticides.[7]

A number of microorganisms have been reported to utilize parathion[4,6,8–10] and its analog methyl parathion.[1,5,11,12] Of these, phosphotriesterase (also known as parathion hydrolase) from *Pseudomonas diminuta* GM[13] is a member of the organophosphorus hydrolases (OPH) and has been studied more extensively[14–22] than methyl parathion hydrolase (MPH, E.C.3.1.8.1) from *Pseudomonas putida*[5] and *Plesiomonas* sp. M6.[11]

A methyl parathion-degrading bacterial strain, *Pseudomonas* sp. WBC-3, was isolated from the soil near Shanongda Pesticides Company in Hubei, China.[23] This bacterium is able to use methyl parathion as a sole C/N source to grow, and also

† Y.-J.D. and M.B. made an equal contribution to this work.

Abbreviations used: MPH, methyl parathion hydrolase; PTE, phosphotriesterase; ROO, rubredoxin:oxygen oxidoreductase; MAD, multi-wavelength anomalous dispersion.

E-mail addresses of the corresponding authors: raozh@xtal.tsinghua.edu.cn; zhangxe@mail.most.gov.cn

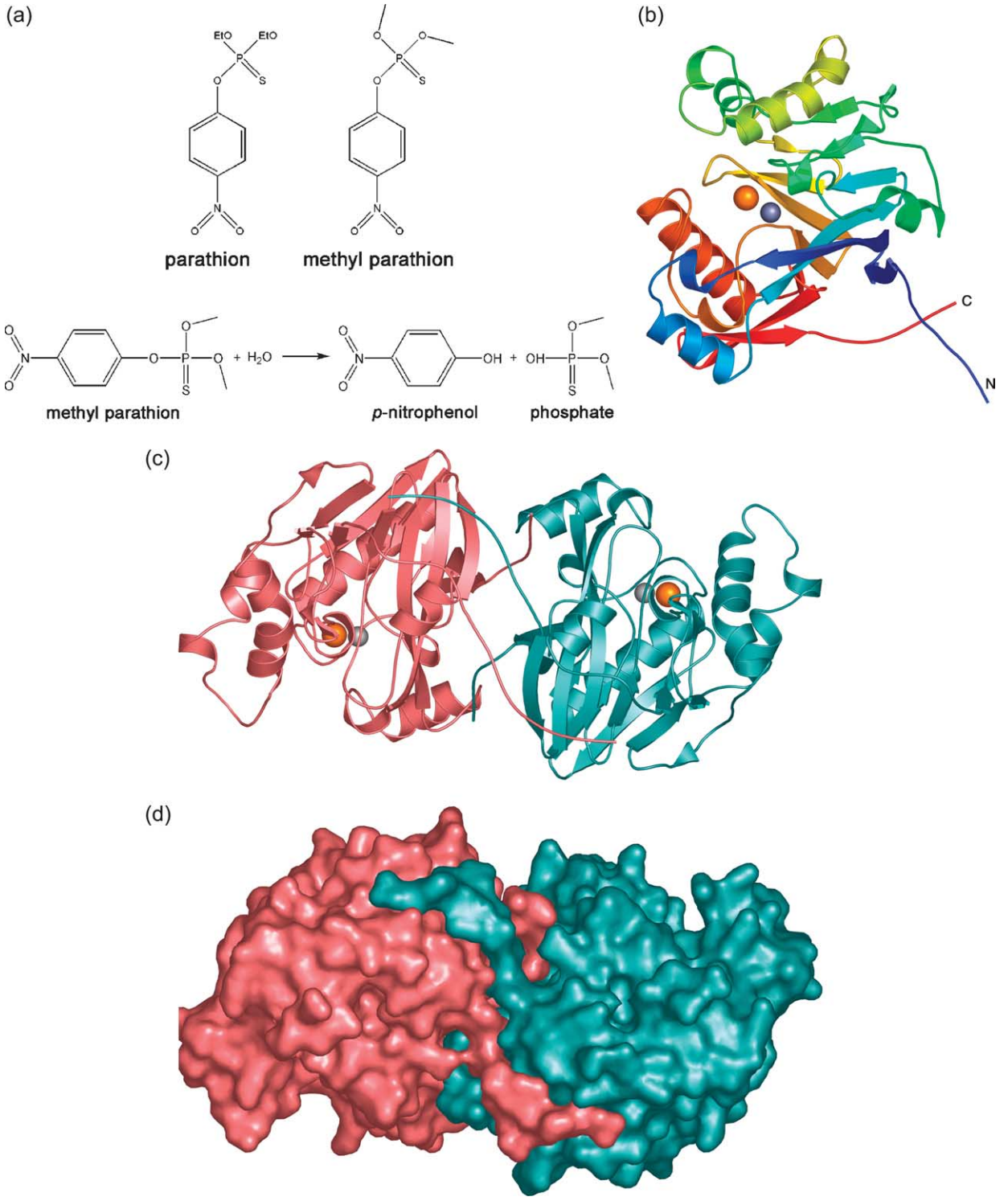

Figure 1. (a) The chemical structures of parathion and methyl parathion, and the reaction for the hydrolysis of methyl parathion. (b) A cartoon representation of the monomer structure of MPH. The structure is colored from blue at the N terminus to red at the C terminus. The two metal ions are shown as silver (Zn) and gold (Cd) spheres. (c) A cartoon representation of the MPH dimer. Protomer A is shown in red and protomer B is shown in blue. The metal ions are shown as silver (Zn) and gold (Cd) spheres. (d) A molecular surface view of the MPH dimer. Coloring is as in (c).

can completely degrade *p*-nitrophenol, the product of methyl parathion.[23] The bacterium contains MPH that can decompose methyl parathion to produce *p*-nitrophenol and phosphate (Figure 1(a)). The *mpd* gene encoding methyl parathion hydrolase from *Pseudomonas* sp. WBC-3 has been determined and the complete gene sequence is now available (GenBank accession number: AY251554). The amino acid sequence deduced from the nucleotide sequence shows 93% and 92% identity with those

Table 1. Data collection and refinement statistics

A. *Data collection statistics*			
Space group	$P4_32_12$		
Unit cell (Å/deg.)	$a=b=85.0$, $c=199.8$, $\alpha=\beta=\gamma=90$		
	MAD peak	MAD edge	Remote
Wavelength (Å)	1.2828	1.2832	0.9000
Resolution limit (Å)	50.0–2.5 (2.59–2.5)	50.0–2.6 (2.69–2.6)	50.0–2.3 (2.38–2.3)
Total reflections	115,659	97,724	180,629
Unique reflections	24,506	22,159	32,143
Completeness	93.0 (73.1)	93.9 (82.7)	95.9 (96.0)
R_{merge}[a] (%)	9.0 (47.9)	9.4 (54.5)	8.0 (38.0)
$\langle I/\sigma(I)\rangle$	7.9 (2.3)	7.5 (1.8)	7.7 (2.5)
B. *Refinement statistics*			
Resolution range	30.0–2.4		
R_{work}[b] (%)	21.4		
R_{free}[b] (%)	25.4		
r.m.s. deviation			
Bond lengths (Å)	0.01		
Bond angles (deg.)	1.67		
Average B factor (Å^2)			
Protein	21.28		
Water	29.35		
Ramachandran plot			
Most favored (%)	87.0		
Generously allowed (%)	11.6		
Additionally allowed (%)	0.8		
Disallowed (%)	0.6		

[a] $R_{merge} = \Sigma_i \Sigma_j |I_j - \langle I\rangle| / \Sigma_i \Sigma_j \langle I\rangle$, where $\langle I\rangle$ is the mean of the intensities of all observations of reflection i; I_j is the intensity of the jth observation of reflection i.

[b] $R_{work} = \Sigma(||F_p(obs)| - |F_p(calc)||)/\Sigma|F_p(obs)|$; R_{free} = R factor for a selected subset (10%) of the reflections that was not included in prior refinement calculations.

from *P. putida* and *Plesiomonas* sp. M6, respectively. However, *mpd* lacks sequence homology with the *opd* genes encoding parathion hydrolase from *P. diminuta* [13] and *Flavobacterium* sp.[9]

The three-dimensional structure of MPH will increase understanding of the function and mechanism of the enzymatic degradation process of the organophosphate pesticides, including the specific structural properties required for the activity of the enzyme and the structural differences between MPH and other OPH. It should also allow the enzyme to be engineered to introduce desired properties. We had previously crystallized MPH by the hanging-drop, vapor-diffusion method.[24] Here, we report the crystal structure of MPH (PDB code 1P9E) to 2.4 Å resolution, and discuss the structural differences between MPH and the widely studied phosphotriesterase, as well as the specific structural properties required for the activity of the enzyme. Point mutations are introduced to demonstrate the substrate binding characteristics of the enzyme based on a kinetic analysis.

Results and Discussion

Structure determination

The structure of MPH was determined to 2.4 Å resolution by multi-wavelength anomalous dispersion (MAD). The crystal contained two molecules in the asymmetric unit. Following several rounds of NCS averaging, the quality of the experimental electron density map was sufficient such that residues 36–329 of chain A and residues 36–329 of chain B could be traced. No density was observed for residues 1–35 or 330–331, and density was poor for residues 186–195 in each subunit. Stereochemistry for the model is good, with 87.0% of residues in the most favored region of the Ramachandran plot generated using PROCHECK.[25] A small number of residues (0.6%) are located in disallowed regions of the Ramachandran plot, but these lie in disordered regions of the structure and could not be modeled easily. The final model consists of 586 residues, 176 water molecules, two Zn^{2+}, two Cd^{2+}, and 12 glycerol molecules. Data collection and refinement statistics are summarized in Table 1.

Structural overview

The structure of MPH is a homodimer comprising of two crystallographically independent subunits. The monomer structure of MPH can be described as an αβ/βα sandwich typical of the metallo-hydrolase/oxidoreductase fold. Two internal mixed β-sheets are flanked either side by three solvent-exposed α-helices. Each subunit is composed of a β-lactamase-like domain, which includes the binuclear metal center. The binuclear metal site is located between the two β-sheets and is surrounded by two αβ-loops.

Dimer structure

The MPH structure forms an intimate, symmetric 2-fold dimer as shown in Figure 1. The dimer interface is formed by the N-terminal arm, the α2 helix, strands β3, β14 and β15, and the C-terminal arm of each subunit. Hydrogen bonds are mediated by the residues Ala36, Val40, Arg41, Thr42, Ser43, Arg49, Glu56, Lys86, Glu94, Tyr135, Gln139, Asp141, Glu314, Arg319, Tyr325, Ser326, Val327 and Val328. The dimer buries a total surface area of 1881 Å^2.

The N-terminal arm of each subunit appears to play a significant role in dimerization. The arm of one subunit binds into a groove on the surface of its partner subunit. Hydrogen bonds are made between the N-terminal arm (residues 36–56) and residues located in the loop between α3 and β5, including Tyr135, Gln139 and Asp141. The result of this dimer interaction may be to provide structural stability to the metal binding center, since several coordinating residues (His147, His149, Asp151 and His152) are located on the loop between β5 and α4.

Determination of the Zn^{2+}/Cd^{2+} metal binding positions

The presence of zinc in the MPH enzyme was previously confirmed by inductively coupled plasma mass spectrometry (ICP-MS) and X-ray absorption fine structure (XAFS) analysis (data not shown). It was expected that the asymmetric unit of MPH would contain four zinc ions in two molecules. When we came to locate the ions from the experimentally determined electron density map, however, it became apparent that the two ions in each subunit were not equivalent from their peak heights. MPD could be crystallized only in the presence of $CdCl_2$, so we surmised that the addition of divalent cations caused one of the zinc ions to be replaced by cadmium for the following reasons. At the experimentally determined peak wavelength of 1.2828 Å for zinc, the anomalous scattering coefficient $\Delta f''$ is ~3.9 for zinc and ~3.4 for cadmium. Calculation of an anomalous difference electron density map confirmed the location of two metal ions in protomer A, with respective peak heights of 16.1 for the more buried ion and 12.0 for the less buried ion. Similarly, in protomer B, the respective peak heights of the two metal ions were 16.1 for the more buried ion and 10.2 for the less buried ion. Refinement with two Zn^{2+} per subunit resulted in a slightly higher crystallographic R-factor (R_{work} = 21.7%, R_{free} = 25.5%). In subunit A, the B-factors of the Zn^{2+} α-metal and Cd^{2+} β-metal are 21.7 Å^2 and 27.0 Å^2, respectively. In subunit B, the B-factors of the Zn^{2+} α-metal and Cd^{2+} β-metal are 19.4 Å^2 and 29.1 Å^2, respectively. If the structure is refined with Zn^{2+} in the β-metal positions, the B-factors reduce to 9.1 Å^2 for subunit A and 15.6 Å^2 for subunit B. From these results, we conclude that the more buried ion (α-metal) is Zn^{2+} and the more solvent-exposed ion (β-metal) is Cd^{2+}. This phenomenon of metal substitution has previously been observed for phosphotriesterase, without any loss of enzymatic activity.[21]

Metal center

The MPH structure includes a binuclear metal center located between the inner β-sheets of the αβ/βα sandwich. The two ions are separated by a distance of 3.5 Å and are coordinated by seven protein residues and two water molecules. Asp255 and a water molecule serve to bridge the two ions together. One of the ions is more buried, and is coordinated by Asp151, His152, Asp255, His302 and the bridging water molecule in an octahedral ligation sphere. The less buried ion is coordinated by His147, His149, His234 and Asp255, as well as the bridging water molecule and a second water molecule. The coordination sphere of the less buried ion is also octahedral (Figure 2(a) and (b)).

The metal centers of protomers A and B are identical. In the metal center of both protomers, the less tightly bound ion (or β-metal) is replaced by cadmium, resulting in a mixed hybrid binuclear center. The larger Cd^{2+} creates space for an additional sixth co-ordination ligand, which is occupied by a water molecule. This is consistent with observations for phosphotriesterase, where a similar phenomenon of metal substitution has been observed in which both zinc ions can be replaced by cadmium, manganese, cobalt or nickel without any resulting conformational changes or loss of enzyme activity.[21] This would suggest that even with a mixed hybrid binuclear metal center, MPH is still catalytically competent.

Located near the metal center of each molecule is an oval-shaped piece of electron density, which we have modeled as a glycerol molecule since glycerol was added as a cryoprotectant (Figure 2(d)). The O2 atom of glycerol sits about 3.8 Å from the Zn^{2+}. In molecule A, the glycerol molecule forms a hydrogen bond with a single water molecule, which in turn makes a hydrogen bond with Phe196. Hydrophobic contact is also made with Leu67. In molecule B, the glycerol molecule makes hydrogen bonds with two water molecules *via* the O3 atom, and a hydrophobic contact with Leu67. The presence of a cavity (occupied by glycerol) near the metal binding center of each subunit suggests the location of a substrate-binding site. The environment of the putative binding site is hydrophobic and includes several pockets lined by hydrophobic residues, including Leu65, Leu67, Phe119, Trp179, Phe196, Leu273 and Leu258. In particular, modeling of the methyl parathion substrate into this cavity suggests that Phe119 and Phe196 are ideally placed to anchor the phenyl group of methyl parathion (data not shown).

To investigate the contribution of the aromatic amino acids present at the entrance of the catalytic pocket to the binding of the substrate, six single substitutions, W179F, W179A, F196W, F196A, F119W and F119A, were constructed using overlap

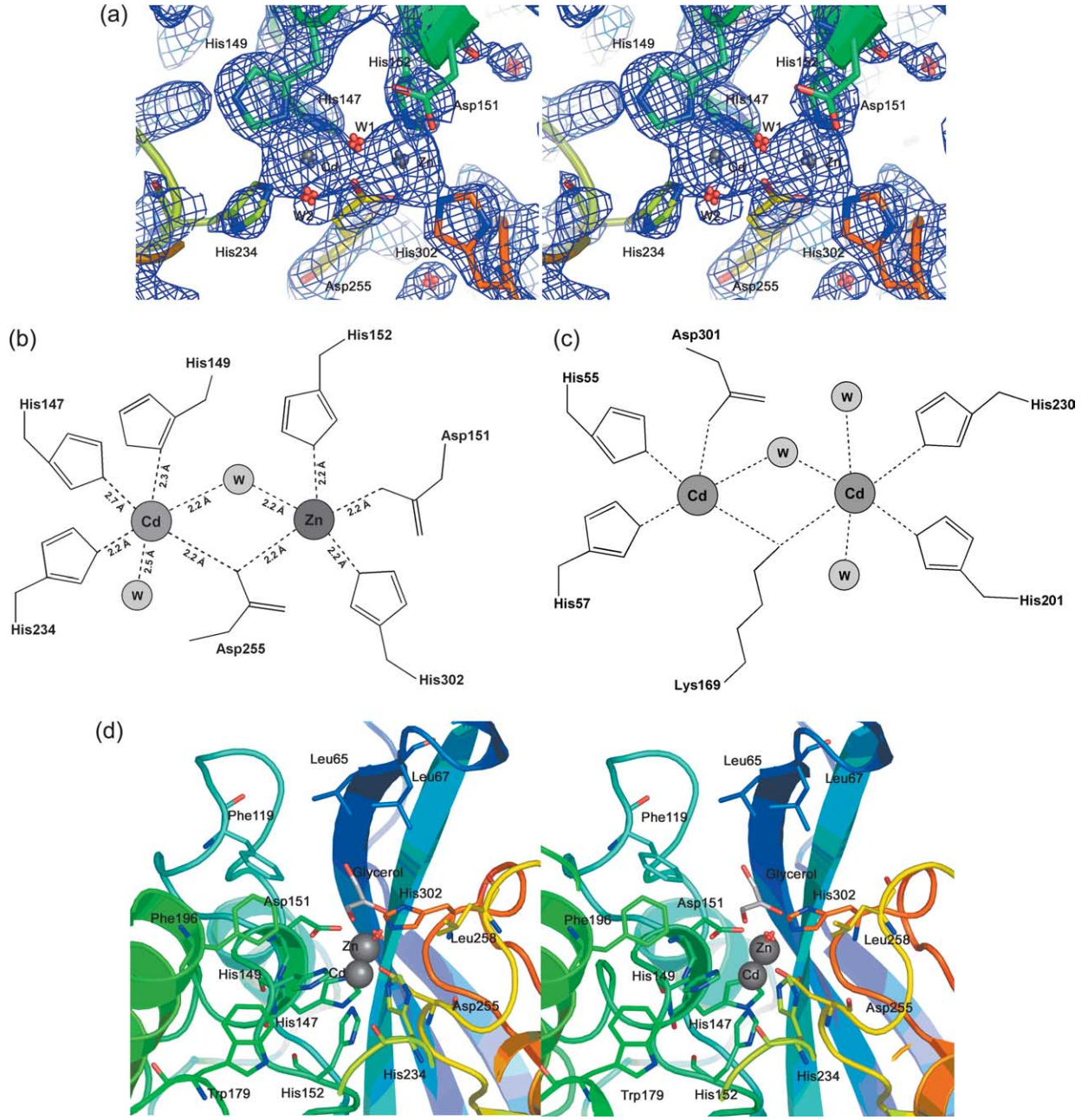

Figure 2. (a) A stereo Figure showing electron density covering the metal center. A composite omit map contoured at 1.5σ is shown covering the metal center. The two metal ions are shown as grey spheres. The seven metal-coordinating residues are shown and labeled. The bridging water (W1) and additional water molecule (W2) are also shown. The coloring is as in Figure 1(b). (b) A schematic showing the mixed-hybrid metal center of MPH. Broken lines represent hydrogen bonds. Hydrogen bonding distances are given as average values for the two molecules. (c) A schematic showing the metal center of phosphotriesterase (PTE) with two Cd^{2+}. Broken lines represent hydrogen bonds. (d) The active site of MPH, showing the metal binding center. Active site residues that might be involved in substrate binding (Leu65, Leu67, Phe119, Trp179, Phe196 and Leu258) are also shown and labeled.

PCR extension techniques, and kinetic experiments were performed. As shown in Table 2, K_m of W179A and F196A increased two- and threefold, respectively, whereas their k_{cat} markedly decreased, indicating that replacement of tryptophan and phenylalanine by alanine at positions 179 and 196 results in decreased affinity of the enzyme for the substrate. Mutating phenylalanine to alanine at position 119 (F119A) also caused an increase of K_m and decrease of k_{cat}, which further suggests that the aromatic amino acids in this particular region contribute to the affinity for methyl parathion. Interchange mutations (W179F and F196W) had different effects on the enzyme kinetics: k_{cat}/K_m for W179F decreased to some extent while k_{cat}/K_m for F196W remained almost unchanged. On the other hand, replacement of phenylalanine by tryptophan resulted in a slight decrease of k_{cat}/K_m compared to

Table 2. Kinetic analysis of MPH and its mutants

Type of MPH	Specific activity (units/mg)	K_m (μM)	k_{cat} (s^{-1})	k_{cat}/K_m (s^{-1} μM^{-1})
Wild-type	50.5	37.4	37.1	0.992
W179F	34.5	48.4	30.6	0.632
W179A	8.4	74.6	7.9	0.106
F196W	64.0	50.0	52.8	1.056
F196A	4.8	107.4	5.0	0.047
F119W	29.2	28.2	20.8	0.734
F119A	32.0	41.1	23.8	0.578

all non-aromatic substitutions. Putting the results together and considering the most favorable substrate of MPH is methyl parathion, which contains a *p*-methyl benzene group, we conclude that the aromatic cluster formed by the amino acid residues Phe119, Trp179 and Phe196 plays a key role in facilitating enzyme-substrate binding and therefore the catalytic process.

Structural comparison with other β-lactamases

A DALI[26] search for structural similarity shows that MPH is homologous with rubredoxin:oxygen oxidoreductase (PDB ID: 1E5D),[27] metallo-β-lactamases from *Bacteroides fragilis* (PDB ID: 1A7T)[28] and *Stenotrophomonas maltophilia* (PDB ID: 1SML),[29] and human glyoxalase II (PDB ID: 1QH5)[30] (Figure 3). Four residues in MPH that are involved in metal coordination form an H-X-H-X-DH sequence motif.

Rubredoxin:oxygen oxidoreductase (ROO) consists of two domains: a β-lactamase domain (residues 1–249) and a flavodoxin-like domain (residues 250–402). MPH is only homologous to the β-lactamase domain of ROO with an r.m.s. deviation of 1.4 Å. ROO is not a Zn(II)-containing enzyme but instead contains a di-iron center for dioxygen reduction. The residues involved in metal coordination in ROO differ slightly from those in MPH, but are in structurally equivalent positions in the two enzymes. ROO has an H-X-E-X-DH sequence motif rather than the H-X-H-X-DH sequence motif of MPH. Interestingly, both iron atoms can be substituted by zinc to form a typical metallo-β-lactamase center if two polarizable ligands are changed to two weakly polarizable ligands, suggesting an evolutionary relationship between ROO and bacterial metallo-β-lactamases.

Metallo-β-lactamases are Zn(II)-containing enzymes that hydrolyze the β-lactam bond in penicillins, cephalosporins, and carbapenems, and are involved in bacterial antibiotic resistance. The metallo-β-lactamases from *B. fragilis* and *S. maltophilia* can both be superimposed with MPH, with respective r.m.s.d. of 1.4 Å and 1.5 Å. Structural alignment shows that all metal-coordinating residues are conserved between MPH and the metallo-β-lactamases, with the exception of the bridging residue Asp255. Instead, *B. fragilis* metallo-β-lactamase contains a serine (Ser185), while *S. maltophilia* metallo-β-lactamase contains a cysteine residue (Cys164) and a water molecule together in the equivalent position.

Human glyoxalase II belongs to the glyoxalase system, which catalyzes the conversion of toxic

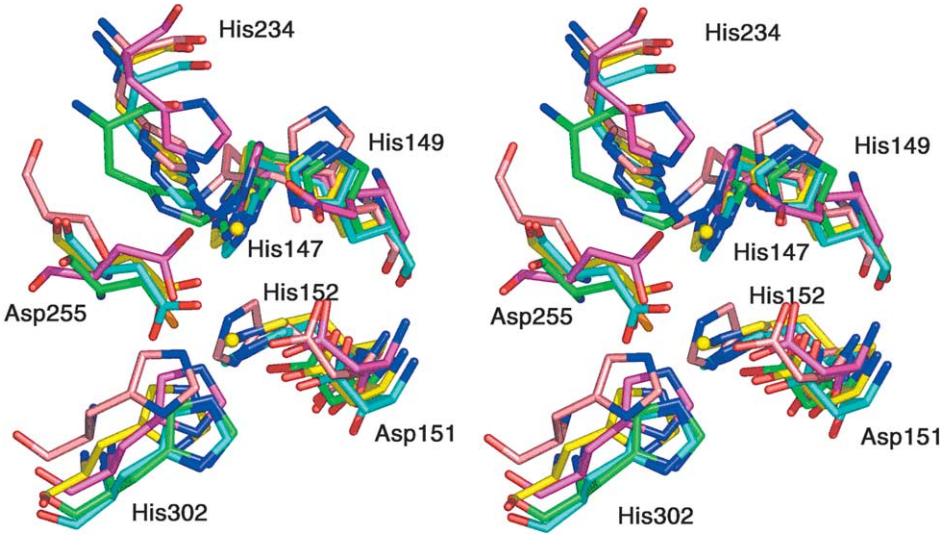

Figure 3. Superposition of metal centers. Structural homologs of MPH were identified using DALI (www.ebi.ac.uk/dali/). The color key is as follows: MPH, yellow; ROO (1E5D), magenta; metallo-β-lactamase (1A7T), green; metallo-β-lactamase (1SML), salmon; human glyoxalase II (1QH5), cyan.

2-oxoaldehydes to 2-hydroxycarboxylic acids using glutathione (GSH) as a coenzyme.[31] The structure of human glyoxalase II is composed of two domains: the four-layered β-sandwich of the metallo-β-lactamase domain, and a smaller α-helical domain. Its metallo-β-lactamase domain can be superimposed with MPH with an r.m.s.d. of 1.6 Å. All metal coordinating residues are conserved between MPH and human glyoxalase II.

Structural comparison with parathion hydrolase

Parathion hydrolase, more commonly known as phosphotriesterase (PTE), is remarkable for its extremely broad substrate profile.[32–34] It can catalyze the hydrolysis of many nerve agents (such as sarin, soman, and VX) and organophosphate pesticides, including methyl parathion. The best substrate identified to date is paraoxon, but many modifications can be made to the phosphorus core without any loss of substrate turnover. PTE has been classified as a metallo-dependent hydrolase and possesses an $(\alpha\beta)_8$ TIM barrel structure. The substitution of both zinc ions by cadmium, manganese, cobalt or nickel does not result in any conformational changes or loss of enzymatic activity.[14,21]

MPH shares no sequence or structural homology with PTE. However, there are interesting similarities in their metal centers. Like MPH, bacterial PTE also contains a binuclear zinc center (Figure 2(c)). The two metals are coordinated by four histidine residues (His55, His57, His201, and His230) together with a single carboxylate from Asp301. The two metals are also bridged *via* a carboxylated lysine, Lys169, and a water molecule. In the case of the mixed Zn^{2+}/Cd^{2+} species of PTE, the metal coordination sphere is octahedral, as is the case for the MPH structure reported here.

The binding pockets in PTE have been well defined and are formed by the hydrophobic residues Ile106, Trp131, Ser308, His257, Leu271, Leu303 and Met317.[18] The very hydrophobic environments surrounding the metal centers of MPH and PTE suggest that MPH might also share the broad substrate range of PTE, which is consistent with our previous investigation using pure MPH. Comparing substrate-bound forms of PTE with the MPH structure can provide more information about the active site of MPH, despite the lack of homology between the two structures. From a study of substrate analog binding to PTE, the inhibitor-binding pocket of PTE is characterized by a lack of direct electrostatic interactions between the substrates and the protein.[35] The complex of PTE with diisopropyl methyl phosphonate indicates only one hydrogen bond between Trp131 and the substrate phosphoryl oxygen, while the complex of PTE with triethyl phosphate shows no hydrogen bonds between protein and substrate.[35] In the case of the PTE–diisopropyl methyl phosphonate complex, the ligand is located an average of 2.1 Å from the solvent-accessible β-metal ion, whereas triethyl phosphate is located 3.4 Å from the β-metal. The putative active site of MPH contains a glycerol from the cryoprotectant solution, which is located approximately 3.7 Å from the β-metal and makes only one indirect, water-mediated hydrogen bond with Leu67.

Interestingly, residue Phe306 in the active site of the PTE structure is found to limit the size of the substrate substituent. Mutation of Phe306 to alanine in PTE results in significant loss of enzyme activity for a range of substrates, suggesting that Phe306 is critical for the maintenance of the integrity of the active site and for facilitating enzyme–substrate binding.[35] This is analogous to the aromatic cluster of residues (Phe119, Trp179 and Phe196) that we have identified near the active site of MPH, as discussed previously (Table 2), and may provide an explanation for the similar substrates of both enzymes.

Implications for catalytic mechanism

The overall similarity between the metal centers of MPH and phosphotriesterase suggests some commonality between their catalytic mechanisms. Therefore, we have proposed a mechanism for the hydrolysis of methyl parathion by MPH. The mechanism is based on that proposed by Benning and co-workers from phosphotriesterase structures with paraoxon, an analog of parathion, in the active site.[21] The reaction mechanism is most likely to proceed *via* the attack of the bridging water molecule on the phosphorus center of the bound substrate. The organophosphate would most likely bind to the binuclear metal center within the active site *via* coordination of the phosphoryl oxygen to the β-metal ion, thus weakening the binding of the bridging water to the β-metal. The metal–oxygen interaction would then polarize the phosphoryl oxygen bond, making the phosphorus center more electrophilic. Nucleophilic attack by the bound water would most likely be assisted by abstraction of a proton from one of the coordinating histidine residues. As the hydroxide attacks the phosphorus center, the bond to the leaving group would then be weakened. Further work is needed to confirm the details.

Conclusions

We have successfully determined the structure of methyl parathion hydrolase from *Pseudomonas* sp. WBC 3 to 2.4 Å. Furthermore, the structure confirms MPH to be a member of the metallo-β-lactamase family with significant conservation of the metal coordinating residues in the binuclear metal center. Despite the lack of any sequence or structural homology with phosphotriesterase, there are obvious similarities in their metal-binding centers that suggest a common catalytic mechanism. An aromatic cluster formed by three amino acid residues oriented at the entrance to the catalytic

center plays a key role in enzyme affinity to methyl parathion. This work raises a number of questions to be addressed by further study, such as whether or not MPH shares the same broad substrate specificity of phosphotriesterase. The structure of MPH should allow the enzyme to be engineered to enlarge its substrate range.

Materials and Methods

Cloning, expression, purification and crystallization

The cloning, expression, purification and crystallization of MPH have been described.[24] Briefly, the purified protein was concentrated to 40–50 mg ml^{-1} and immediately used for crystallization. Crystallization trials were conducted at 291 K in 16-well plates using the hanging-drop, vapor-diffusion method. Crystals suitable for X-ray diffraction were obtained from a reservoir solution containing 30% (w/v) PEG400, 0.1 M sodium acetate (pH 4.6), 0.1 M $CdCl_2$.

Data collection

MPH was confirmed to be a Zn-containing enzyme by ICP-MS analysis (data not shown). XAFS analysis was used to determine appropriate wavelengths for Zn-MAD data collection. Data were collected on beamline BL41XU of SPring-8 (Hyogo, Japan) at 100 K, using glycerol as a cryoprotectant. Three datasets were collected at wavelengths corresponding to peak (1.2828 Å), edge (1.2832 Å) and remote (0.9000 Å) energies. Data processing was performed using the program DENZO and data sets were scaled and merged using SCALEPACK.[35]

Structure determination

The structure of MPH was determined by multi-wavelength anomalous diffraction (MAD) using the bound zinc ions. Three out of four expected Zn sites in the asymmetric unit were located using SOLVE,[36] and initial phases were calculated to 3.0 Å. RESOLVE[37] was used for density modification and phase extension to 2.4 Å; however, initial density maps were of generally poor quality and not suitable for tracing the complete structure. We were able to identify secondary structure elements from the electron density, and so the partially traced structure was used to locate 2-fold non-crystallographic symmetry (NCS). Several rounds of NCS averaging were then performed in RESOLVE, resulting in a significant improvement in electron density. Automatic model tracing could be started and a total of 419 residues in two molecules were built by RESOLVE; the remaining residues were built manually in O.[38] Alternate cycles of rebuilding in O and refinement in CNS[39] were subsequently used to reduce the crystallographic *R*-factor and R_{free}. In the final stages of refinement, 176 water molecules were picked from peaks above 3σ in the $|F_o|-|F_c|$ electron density map. Two zinc ions, two cadmium ions and 12 glycerol molecules were also added to the model. For location of the Zn^{2+} and Cd^{2+}, calculation of an anomalous difference electron density map and peak searching were performed using CCP4.

Acknowledgements

This study was supported by the Ministry of Science and Technology (MOST) Human Liver Proteomics Project (grant no. 2004CB520801), the State "863" High-Tech Project (grant no. 2002BA711A12), "973" Project (grant no. G1999075602) and the NSFC (grant no. 30221003).

Supplementary Data

Supplementary data associated with this article can be found, in the online version, at doi:10.1016/j.jmb.2005.08.057

The supplementary data comprises a Figure showing sequence alignments.

References

1. Chaudhry, G. R., Ali, A. N. & Wheeler, W. B. (1988). Isolation of a methyl parathion-degrading *Pseudomonas* sp. that possesses DNA homologous to the opd gene from a *Flavobacterium* sp. *Appl. Environ. Microbiol.* **54**, 288–293.
2. Harper, L. L., McDaniel, C. S., Miller, C. E. & Wild, J. R. (1988). Dissimilar plasmids isolated from *Pseudomonas diminuta* MG and a *Flavobacterium* sp. (ATCC 27551) contain identical opd genes. *Appl. Environ. Microbiol.* **54**, 2586–2589.
3. Hayatsu, M., Hirano, M. & Tokuda, S. (2000). Involvement of two plasmids in fenitrothion degradation by *Burkholderia* sp. strain NF100. *Appl. Environ. Microbiol.* **66**, 1737–1740.
4. Munnecke, D. M. & Hsieh, D. P. (1974). Microbial decontamination of parathion and *p*-nitrophenol in aqueous media. *Appl. Microbiol.* **28**, 212–217.
5. Rani, N. L. & Lalithakumari, D. (1994). Degradation of methyl parathion by *Pseudomonas putida*. *Can. J. Microbiol.* **40**, 1000–1006.
6. Serdar, C. M., Gibson, D. T., Munnecke, D. M. & Lancaster, J. H. (1982). Plasmid involvement in parathion hydrolysis by *Pseudomonas diminuta*. *Appl. Environ. Microbiol.* **44**, 246–249.
7. Cho, T. H., Wild, J. R. & Donnelly, K. C. (2000). Utility of organophosphorus hydrolase for the remediation of mutagenicity of methyl parathion. *Environ. Toxicol. Chem.* **19**, 2022–2028.
8. Mulbry, W. W., Karns, J. S., Kearney, P. C., Nelson, J. O., McDaniel, C. S. & Wild, J. R. (1986). Identification of a plasmid-borne parathion hydrolase gene from *Flavobacterium* sp. by southern hybridization with opd from *Pseudomonas diminuta*. *Appl. Environ. Microbiol.* **51**, 926–930.
9. Mulbry, W. W. & Karns, J. S. (1989). Purification and characterization of three parathion hydrolases from gram-negative bacterial strains. *Appl. Environ. Microbiol.* **55**, 289–293.
10. Sethunathan, N. & Yoshida, T. (1973). A *Flavobacterium* sp. that degrades diazinon and parathion. *Can. J. Microbiol.* **19**, 873–875.
11. Zhongli, C., Shunpeng, L. & Guoping, F. (2001). Isolation of methyl parathion-degrading strain M6 and cloning of the methyl parathion hydrolase gene. *Appl. Environ. Microbiol.* **67**, 4922–4925.
12. Laveglia, J. & Dahm, P. A. (1977). Degradation of

organophosphorus and carbamate insecticides in the soil and by soil microorganisms. *Annu. Rev. Entomol.* **22**, 483–513.
13. Dumas, D. P., Caldwell, S. R., Wild, J. R. & Raushel, F. M. (1989). Purification and properties of the phosphotriesterase from *Pseudomonas diminuta*. *J. Biol. Chem.* **264**, 19659–19665.
14. Omburo, G. A., Mullins, L. S. & Raushel, F. M. (1993). Structural characterization of the divalent cation sites of bacterial phosphotriesterase by 113Cd NMR spectroscopy. *Biochemistry*, **32**, 9148–9155.
15. Kuo, J. M., Chae, M. Y. & Raushel, F. M. (1997). Perturbations to the active site of phosphotriesterase. *Biochemistry*, **36**, 1982–1988.
16. Banzon, J. A., Kuo, J. M., Fischer, D. R., Stang, P. J. & Raushel, F. M. (1995). Histidine-254 is essential for the inactivation of phosphotriesterase with the alkynyl phosphate esters and diethyl pyrocarbonate. *Biochemistry*, **34**, 750–754.
17. Banzon, J. A., Kuo, J. M., Miles, B. W., Fischer, D. R., Stang, P. J. & Raushel, F. M. (1995). Mechanism-based inactivation of phosphotriesterase by reaction of a critical histidine with a ketene intermediate. *Biochemistry*, **34**, 743–749.
18. Vanhooke, J. L., Benning, M. M., Raushel, F. M. & Holden, H. M. (1996). Three-dimensional structure of the zinc-containing phosphotriesterase with the bound substrate analog diethyl 4-methylbenzylphosphonate. *Biochemistry*, **35**, 6020–6025.
19. Benning, M. M., Kuo, J. M., Raushel, F. M. & Holden, H. M. (1994). Three-dimensional structure of phosphotriesterase: an enzyme capable of detoxifying organophosphate nerve agents. *Biochemistry*, **33**, 15001–15007.
20. Benning, M. M., Kuo, J. M., Raushel, F. M. & Holden, H. M. (1995). Three-dimensional structure of the binuclear metal center of phosphotriesterase. *Biochemistry*, **34**, 7973–7978.
21. Benning, M. M., Shim, H., Raushel, F. M. & Holden, H. M. (2001). High resolution X-ray structures of different metal-substituted forms of phosphotriesterase from *Pseudomonas diminuta*. *Biochemistry*, **40**, 2712–2722.
22. Hong, S. B. & Raushel, F. M. (1996). Metal-substrate interactions facilitate the catalytic activity of the bacterial phosphotriesterase. *Biochemistry*, **35**, 10904–10912.
23. Chen, Y., Zhang, X., Liu, H., Wang, Y. & Xia, X. (2002). Study on *Pseudomonas* sp. WBC-3 capable of complete degradation of methylparathion. *Wei Sheng Wu Xue Bao*, **42**, 490–497.
24. Sun, L., Dong, Y., Zhou, Y., Yang, M., Rao, Z. & Zhang, X. E. (2004). Crystallization and preliminary X-ray studies of methyl parathion hydrolase from *Pseudomonas* sp. WBC-3. *Acta Crystallog. sect D*.
25. Laskowski, R. A., MacArthur, M. W., Moss, D. S. & Thornton, J. M. (1993). PROCHECK: a program to check the stereochemical quality of protein structures. *J. Appl. Crystallog.* **26**, 283–291.
26. Holm, L. & Sander, C. (1998). Protein folds and families: sequence and structure alignments. *Nucl. Acids Res.* **26**, 316–319.
27. Frazao, C., Silva, G., Gomes, C. M., Matias, P., Coelho, R., Sieker, L. *et al*. (2000). Structure of a dioxygen reduction enzyme from *Desulfovibrio gigas*. *Nature Struct. Biol.* **7**, 1041–1045.
28. Fitzgerald, P. M. D., Wu, J. K. & Toney, J. H. (1998). Unanticipated inhibition of the metallo-beta-lactamase from *Bacteroides fragilis* by 4-morpholineethanesulfonic acid (MES): a crystallographic study at 1.85 Å resolution. *Biochemistry*, **37**, 6791–6800.
29. Ullah, J. H., Walsh, T. R., Taylor, I. A., Emery, D. C., Verma, C. S., Gamblin, S. J. & Spencer, J. (1998). The crystal structure of the L1 metallo-beta-lactamase from *Stenotrophomonas maltophilia* at 1.7 Å resolution. *J. Mol. Biol.* **284**, 125–136.
30. Cameron, A. D., Ridderstrom, M., Olin, B. & Mannervik, B. (1999). Crystal structure of human glyoxalase II and its complex with a glutathione thiolester substrate analogue. *Structure*, **7**, 1067–1078.
31. Dumas, D. P., Durst, H. D., Landis, W. G., Raushel, F. M. & Wild, J. R. (1990). Inactivation of organophosphorus nerve agents by the phosphotriesterase from *Pseudomonas diminuta*. *Arch. Biochem. Biophys.* **277**, 155–159.
32. Raushel, F. M. (2002). Bacterial detoxification of organophosphate nerve agents. *Curr. Opin. Microbiol.* **5**, 288–295.
33. Raushel, F. M. & Holden, H. M. (2000). Phosphotriesterase: an enzyme in search of its natural substrate. *Advan. Enzymol. Relat. Areas Mol. Biol.* **74**, 51–93.
34. Benning, M. M., Hong, S. B., Raushel, F. M. & Holden, H. M. (2000). The binding of substrate analogs to phosphotriesterase. *J. Biol. Chem.* **275**, 30556–30560.
35. Otwinowski, Z. & Minor, W. (1997). Processing of X-ray diffraction data collected in oscillation mode. *Methods Enzymol.* **276**, 307–326.
36. Terwilliger, T. C. & Berendzen, J. (1999). Automated MAD and MIR structure solution. *Acta Crystallog. sect. D*, **55**, 849–861.
37. Terwilliger, T. C. (2000). Maximum-likelihood density modification. *Acta Crystallog. sect. D*, **56**, 965–972.
38. Jones, T. A., Zou, J. Y., Cowan, S. W. & Kjeldgaard, M. (1991). Improved methods for building protein models in electron density maps and the location of errors in these models. *Acta Crystallog. sect. A*, **47**, 110–119.
39. Brunger, A. T., Adams, P. D., Clore, G. M., DeLano, W. L., Gros, P., Grosse-Kunstleve, R. W. *et al*. (1998). Crystallography, NMR system: a new software suite for macromolecular structure determination. *Acta Crystallog. sect. D*, **54**, 905–921.

Edited by R. Huber

(Received 6 June 2005; received in revised form 21 August 2005; accepted 24 August 2005)
Available online 8 September 2005